STUDY ON FLOW AND HEAT TRANSFER CHARACTERISTICS OF COOLING CHANNEL FILLED WITH X-SHAPED TRUSS ARRAY

by

Lei XI, Liang XU*, Jianmin GAO, Zhen ZHAO, and Yunlong LI

State Key Laboratory for Manufacturing Systems Engineering, School of Mechanical Engineering, Xi'an Jiaotong University, Xi'an, Shaanxi, China

Original scientific paper
https://doi.org/10.2298/TSCI220302110X

In order to enhance the cooling performance of turbine blades, novel cooling channels filled with X-shaped truss array were investigated in this study. The flow mechanism and heat transfer characteristic of the cooling channel filled with X-shaped truss array were analyzed numerically. The empirical correlations of friction coefficient and Nusselt number related to the inlet Reynolds number (10000-60000) and truss rod inclination angle (30-45°) were fitted. The results show that the secondary flow vortex in the channel and the Nusselt number on the channel wall both show periodic distributions along the streamwise direction. The row-averaged Nusselt number and friction coefficient of the channel first decrease quickly and then decrease slowly along the streamwise direction. When truss rod inclination angle increases from 30-60°, the whole-averaged Nusselt number and the whole friction coefficient of the channel increase by 25.4-52.3% and 1.19-1.33 times, respectively under different Reynolds number. The channel with truss rod inclination angle of 45° has the best comprehensive thermal performance. In all cases, the ratio of heat transfer quantity of the truss rod surface to the total heat transfer quantity of the channel ranges from 22.9-42.3%. The increase of Reynolds number improves the heat transfer quantity of the channel wall and the increase of truss rod inclination angle reduces the heat transfer quantity of the channel wall.

Key words*: turbine blade, X-shaped truss array, cooling channel, mechanism and characteristics, flow and heat transfer*

Introduction

The operating conditions of heavy-duty gas turbine blades is very harsh [1, 2]. It is urgent to use high efficiency cooling technology with high structural strength to ensure the safe and reliable operation of blades. Truss structure is a kind of multifunctional topology optimization structure [3]. With the development of 3-D printing technology, truss structure has been gradually applied to many industrial fields [4, 5]. Common truss units that make up the truss structures include Kagome-type truss unit, pyramid-shaped truss unit and tetrahedron-shaped truss unit [6]. Advantages of truss structures include high specific strength, high toughness, high specific stiffness and other exceptional mechanical performance, which have been proved by a large amount of [7-10]. Meanwhile, truss structures also have excellent heat conductivity and convective heat transfer capacity [11]. Therefore, if truss structures are filled into the gas turbine blades internal cooling channels, the cooling performance and structural strength of gas turbine blades would be significantly enhanced in prospect.

* Corresponding author, e-mail: xuliang@mail.xjtu.edu.cn

Much literature is available on the thermal performance and cooling performance of truss array structures since 2003. Feng *et al.* [12] experimentally studied the influence of brazing on the thermal and mechanical performance of the wire-woven Kagome truss structure. They found that the brazing can greatly improve the heat dissipation capability of the wire-woven Kagome-type truss structure, but almost do not affect the equivalent heat conductivity of it. Qu *et al.* [13] investigated the equivalent heat conductivity coefficient of an octet-truss unit and obtained the functional relationship among the equivalent heat conductivity of truss unit, porosity, heat conductivity of solids, and other topological parameters. Wei *et al.* [14] obtained the equivalent thermal conductivity of a non-metallic Pyramidal-type truss array structure under different boundary conditions by experimental methods. Yan *et al.* [15] pointed out that the sandwich panels filled with *X*-type truss array and Kagome-type truss array have higher heat transfer performance. Zhang *et al.* [16] stated that for the sandwich panels filled with tetrahedral truss structure, the heat transfer performance of the brazed sandwich panel and casted sandwich panel is nearly the same. The results reported by Jin *et al.* [17] show that the *X*-type truss array structure has more advantages than the Pyramidal-type truss array structure in heat transfer capacity and comprehensive thermal performance. Bai *et al.* [18] also estimated the equivalent heat conductivity coefficient of curved truss structure by numerical and theoretical investigations. Yang *et al.* [19] reported that the average Nusselt number of sandwich panel filled with Kagome truss structure is 8-37% higher than that filled with tetrahedral truss structure. Vaissier *et al.* [20] proposed a new optimization design method to improve the thermal dissipation capacity of graded truss structures, and the method was validated by several case studies. Hou *et al.* [21] reported that the different arrangement directions of the Kagome-type truss structure in the channel can cause a maximum difference of 9.7% in heat transfer coefficient and 20% in friction coefficient. Ekade *et al.* [22] suggested that the octet truss structures are suitable for designing the multifunctional heat exchangers. Chaudhari *et al.* [23] examined the heat conduction, heat transfer and flow performance of octet truss structures by experimental measurement, and pointed that the octet truss structures have excellent multifunctional features. Kaur *et al.* [24] pointed out that the Nusselt number of the endwall of channel filled with octet truss structure is 2.96 times that of the endwall of smooth channel.

In recent years, several researchers propose to apply truss array structures to the internal cooling channel of turbine blade to improve its cooling efficiency. The United Technology Company earlier reported the design concept of internal cooling channel filling rod structures for turbine blade in a patent in [25]. Then, Xu *et al.* [26] experimentally and numerically investigated the mechanical properties and the heat transfer capacity of the typical truss array structure under the cooling conditions of turbine blade, and stated that the mechanical properties and heat transfer capacity of *X*-shaped truss array structure are the best. Liang *et al.* [27] researched the effect of truss unit type on the heat transfer performance and flow characteristics of turbine blade internal channels with different truss array. They suggested that the heat transfer capacity of the body centered cubic array is the best. The authors of the present study previously researched the influence laws of truss rod diameter, transverse spacing ratio and streamwise spacing ratio on the cooling effect of the channels filled with *X*-shaped truss array, and obtained the corresponding optimal parameter combination [28, 29].

According to the aforementioned literature review, although much research has been conducted on the heat transfer and flow characteristics of channels with different truss arrays, little attention has been devoted to the practicability of truss array for the cooling design of turbine blades. The cooling mechanisms and characteristics of the cooling channels filled with truss arrays under the sizes and working conditions of turbine blades are not clear yet and need further investigations.

In view of the aforementioned problems, novel cooling channels filled with *X*-shaped truss array for application gas turbine blade mid-region was investigated in the present work. The flow mechanism and heat transfer characteristic of the channels filled with *X*-shaped truss array were mainly analyzed numerically. The empirical correlations of friction coefficient, f_H, and Nusselt number, $Nu_{H,ave}$, related to the inlet Reynolds number, (Re_H, 10000-60000) and truss rod inclination angle (β, 30-45°) were fitted by the least square method. The findings in the work are meaningful to the design of internal channels filled with *X*-shaped truss cooling structure in heavy-duty gas turbine blades.

Numerical approaches

Numerical model

The cooling channel studied in this work is modeled from an F-class gas turbine blade [29]. The channel length, L, height, H, and wall thickness, δ, are 200 mm, 20 mm, and 1 mm, respectively. Six rows of *X*-shaped truss units are periodically disposed on the channel heated walls along the streamwise direction. The truss rod diameter, d is 4 mm, the streamwise spacing, L_s, between adjacent truss units are 30 mm. The inclination angle of truss rod, β is 30°, 45°, and 60°, which belongs to an optimal parameter range obtained through several numerical simulation tests. The numerical model of the *X*-shaped truss array channel is presented in fig. 1, which is mainly consist of a fluid domain and a solid domain. The two sidewalls of the numerical model were specified as the translational periodicity interface. The bottom wall and the top wall of the solid channel was specified as heated walls. The fluid-solid interfaces between the fluid domain and the solid domain were set as coupling surfaces. In order to make the air-flow fully developed in the front of the test section as well as eliminate the influence of backflow on the numerical results, two smooth channels with the length of 200 mm were added before and behind the truss array channel.

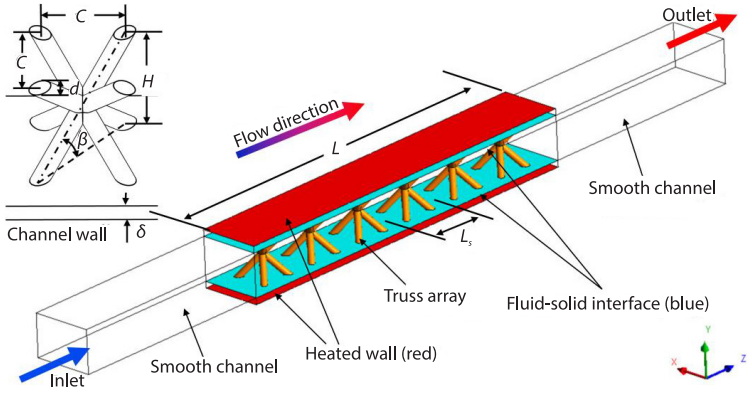

Figure 1. Numerical calculation model of channel filled with *X*-shaped truss array structure

Coupled heat transfer numerical method

In this work, the coupled heat transfer numerical method was used to simulate the flow and heat transfer characteristics of cooling channels filled with *X*-shaped truss array [30, 31]. In the numerical calculations (by CFX), the cooling air was assumed as 3-D, steady, turbulent, incompressible and agravic. The finite volume method was selected to calculate the governing equations of energy, mass and momentum. The RANS equations were adopted to solve the turbulent momentum equations. The bounded central difference scheme with high

resolution was adopted to discretize the governing equations. The SST k-ω turbulence model with near-wall model approach were used to calculate the turbulent flow in the channel due to the accurate prediction of SST k-ω in the cooling performance of truss array channels, as the authors have reported in references [28, 29]. For the heat conduction in the solid channel, only the conduction equation was calculated. Then the same temperature and heat flux were transmitted from the solid channel to the air-flow by the fluid-solid interface with matched grids. When all the residuals were lower than 10^{-6}, the numerical simulations were terminated. In addition, the cooling air enters along the channel inlet normal direction, the inlet Reynolds number is 10000 to 60000, the inlet temperature and turbulence intensity are 298.15 K and 5%. The outlet average static pressure is 101 kPa. The outer surfaces of the top and bottom walls were heated by a constant heat flux of 3000 W/m^2.

The unstructured grid models of X-shaped truss array channels were generated in the Meshing module of Workbench, which are displayed in fig. 2. Prismatic meshes were generated for the channel walls and the truss rod surfaces, so as to simulate the flow and thermal boundary-layers at those regions. In order to ensure $y^+ \leq 1$, the initial height of prismatic meshes was selected as 0.001 mm, the height ratio of prismatic meshes was selected as 1.2, and the layer number of prismatic meshes was selected as 15. Additionally, for enhancing the precision of numerical calculation results, the tetrahedral meshes at and near the truss rods were refined and smoothed repeatedly for both the solid and fluid domains. The grid independence test was carried out to ensure the reliability and economy of the numerical simulations. The results show that the total mesh number 8.6 million for maximum mesh unit size of 0.5 mm can meet the requirements of grid independence test, as the authors have reported in reference [29].

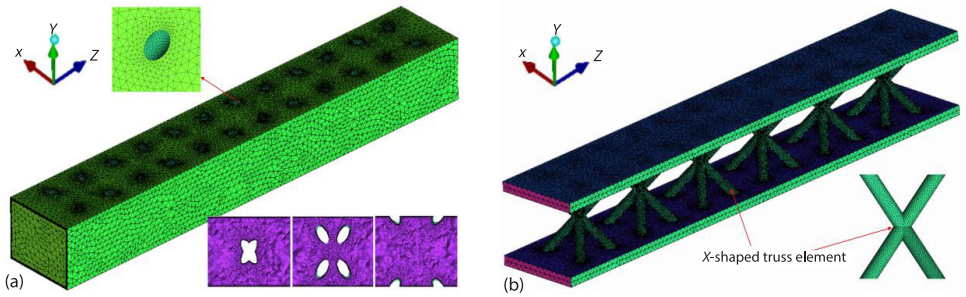

Figure 2. Numerical model of *X*-shaped truss array channel; (a) fluid domain and (b) solid domain

Table 1 shows the comparison between the numerically calculated $Nu_{H,ave}$ by SST k-ω and the experimentally measured $Nu_{H,ave}$ [29] for the channel filled with X-shaped truss array at $\beta = 45°$, so as to verify the reliability of the numerical method. The results show that

Table 1. Comparison of experimental results and numerical results ($\beta = 45°$)

Results of experiment		Results of SST k-ω	
Re	$Nu_{H,ave}$	$Nu_{H,ave}$	Deviations [%]
10000	123.96	108.20	–12.71
20000	165.04	156.23	–5.33
30,000	216.64	206.14	–4.85
40000	242.33	237.81	–1.87
50000	270.39	256.52	–5.13

the numerically calculated $Nu_{H,ave}$ by SST k-ω is in good agreement with the experimentally measured Nu_H. The maximum prediction deviation and mean deviation of $Nu_{H,ave}$ calculated by SST k-ω are –12.71% and –5.97%, respectively. Therefore, the adopted numerical method with SST k-ω model in this investigation for the cooling behavior prediction of the channel filled with X-shaped truss array is suitable and reliable.

Parameter definition

Based on the channel height [28], the channel inlet Reynolds number, Re_H, the local Nusselt number, Nu_H, of channel wall, as well as the channel friction coefficient, f_H, can be defined:

$$\mathrm{Re}_\mathrm{H} = \frac{uH}{\nu} \tag{1}$$

$$\mathrm{Nu}_\mathrm{H} = \frac{qH}{(T_\mathrm{w} - T_\mathrm{f})\lambda} \tag{2}$$

$$f_\mathrm{H} = \frac{\Delta pH}{\frac{\rho S u^2}{2}} \tag{3}$$

where ν, u, ρ, and λ are the kinematic viscosity, inlet velocity, density, and local thermal conductivity of the coolant and q is the heat flux, T_w – the local wall temperature, T_f – the local average temperature of coolant, S – the length of the region of a row truss unit or the whole channel, and Δp – the corresponding pressure drop.

The comprehensive thermal coefficient, G_H, can be calculated:

$$G_\mathrm{H} = \frac{\mathrm{Nu}_\mathrm{H,ave}}{f_\mathrm{H}^{1/3}} \tag{4}$$

where $Nu_{H,ave}$ is the average Nusselt number.

The heat transfer quantity, η_Q, can be calculated:

$$\eta_\mathrm{Q} = \frac{\int_0^{S_\mathrm{inf}} q}{q_\mathrm{ave} S_\mathrm{w}} \times 100\% \tag{5}$$

where S_w is the area of channel outer wall, S_{inf} – the area of the fluid-solid interface, such as the area of the channel inner wall or the total area of truss rod surface, and q_{ave} – the average heat flux given for the channel outer wall.

Results analysis and discussion

Analysis of flow and heat transfer mechanism

Figure 3 illustrates the flow field distributions in the channel filled with X-shaped truss array at $\beta = 45°$. As shown in fig. 3, for the flow field distribution on the section of $y/H = 0.5$ (middle section), the four truss rods meet at the middle section of the channel to form a large quasi circular bar, therefore, the flow field of the middle section is roughly the same as that of the straight cylinder. Specifically, the incoming flow sweeps over the quasi circular bar and forms a horseshoe vortex around the quasi circular bar. Meanwhile, a wake region with a gradually larger range is formed downstream of the quasi circular bar. Due to the blocking effect of

the quasi circular bar, the velocity of the fluid directly behind the quasi circular bar decreases apparently, and the velocity of the fluid on both sides of the quasi circular bar increases rapidly. On the section of $y/H = 0.75$, horseshoe vortexes and wake regions are formed around the four truss rods. The difference is that the horseshoe vortexes and wake regions formed around the two truss rods upstream are larger and slightly offset to the inside of the channel, while the vortexes and wake regions formed around the two truss rods downstream are smaller and slightly offset to the outside of the channel, when compared with the flow field distribution on the section of $y/H = 0.5$. Besides, on the section of $y/H = 0.75$, the flow velocity downstream of each truss rod is low, while the flow velocity on both sides of the truss rod is high, which leads to the lower flow velocity downstream of the *X*-shaped truss unit and the higher flow velocity on both sides of the *X*-shaped truss unit. On the section of $y/H = 0.99$ (near the wall), the flow field distribution on which is similar to that on the section of $y/\mathrm{H} = 0.75$. The difference is that for the flow field distribution on the section of $y/H = 0.99$, the horseshoe vortexes formed around the four truss rods have higher velocity, the vortexes and wake regions around the truss rods are obviously deflected to the inner side of the channel.

For the 3-D vortex core distribution around a single *X*-shaped truss unit, the secondary flow of cooling air along each inclined truss rod can be clearly observed. Specifically, the cooling fluid first impacts the front end of the truss rod and forms small horseshoe vortexes at the front end of the four truss rods. Then the cooling air-flows along the inclined direction of the truss rod. The accumulation of cooling air at the intersection of the four truss rods results in a large horseshoe vortex formed at the middle section ($y/H = 0.5$) of the channel. With the further flow of the cooling air along the inclined truss rod, a large horseshoe vortex is formed near the channel wall at the rear end of each truss rod. Additionally, it can be also seen from fig. 3 that the velocity of horseshoe vortexes around the truss rod of the first row of truss units is slightly higher than that of the vortexes around the subsequent rows of truss units. From the second row of truss units, the distribution patterns of vortexes around each row of truss units remain unchanged.

Figure 4 illustrates the local heat transfer distributions in the channel filled with *X*-shaped truss array at $\beta = 45°$. As displayed in fig. 4, the overall heat transfer effect on the channel wall in the surrounding area of the truss rod is higher due to the flow disturbance effect of *X*-shaped truss unit. The $\mathrm{Nu_H}$ of the channel wall on both sides of the truss rod is higher, while the $\mathrm{Nu_H}$ of the channel wall in the middle of the truss unit is lower, which may be caused by the obstruction effect of the truss unit to the cooling air-flow. Additionally, the upwind surface of truss rod has a high $\mathrm{Nu_H}$ due to the direct impact and wash of cooling air. The heat transfer effect of the downwind surface of the truss rod is rapidly worse due to the influence of the wake flow behind the truss rod. Especially, the heat transfer effect on the position of truss crossing area as well as the position of the truss rod surface near the channel wall is further worse. Besides, the $\mathrm{Nu_H}$ on the truss rod surface is significantly higher than that of the channel wall. It can be also seen from fig. 4 that, due to the entrance effect, the thermal boundary-layer and the flow boundary-layer formed near the channel wall are very thin when the cooling air just enters the channel. Therefore, the $\mathrm{Nu_H}$ on the channel wall at the channel entrance is very high. Then, with the development of the cooling flow, the thermal boundary-layer and the flow boundary-layer formed near the channel wall become thicker rapidly, which results in the rapid increase of heat transfer resistance of the fluid near the wall and leads to the rapid decrease of $\mathrm{Nu_H}$ along the mainflow direction. Then, when the cooling air encounters the truss rods, the horseshoe vortexes appear at the truss rod ends and the wake vortexes are formed downstream of the truss rods. These vortexes seriously break the thick boundary-layer formed on the channel wall and reduce

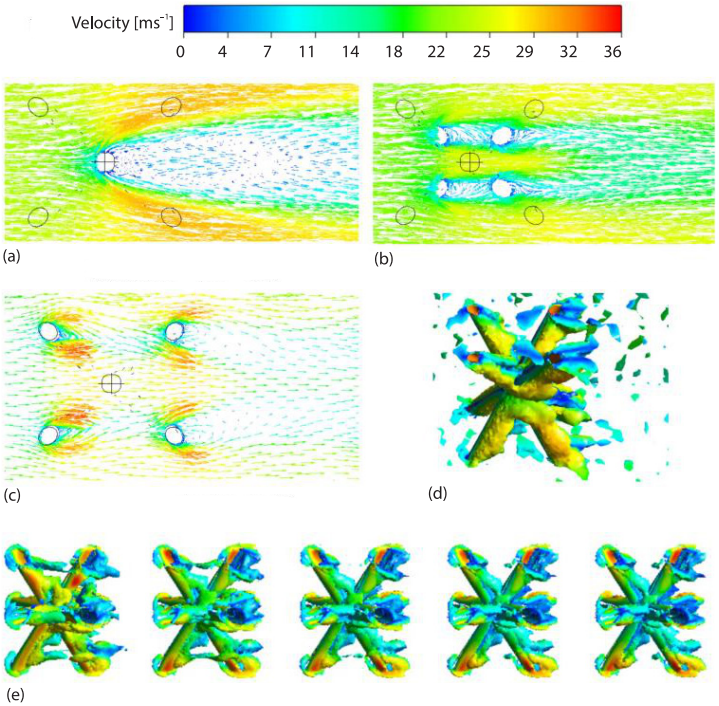

Figure 3. Flow field distributions at $\beta = 45°$; (a) section on $y/H = 0.5$, (b) section on $y/H = 0.75$, (c) section on $y/H = 0.99$ (d) 3-D vortex core, and (e) $Re_H = 30000$ and $\beta = 45°$

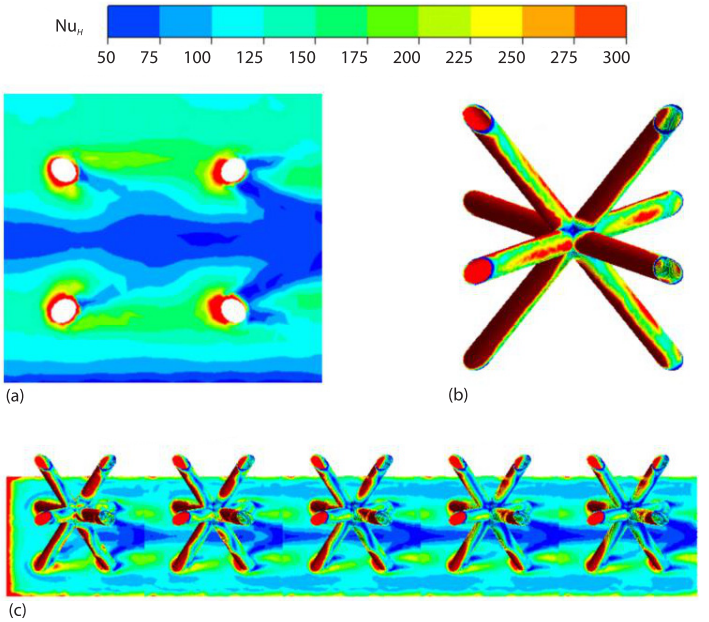

Figure 4. Local heat transfer distributions at $\beta = 45°$; (a) channel wall, (b) truss rod surface, and (c) $Re_H = 30000$ and $\beta = 45°$

the heat transfer resistance between the channel wall and the cooling air, and then enhance the local heat transfer effect of the channel wall. Due to the periodic arrangement of truss units, the Nu_H on the channel wall shows the periodic similar distribution along the mainflow direction. Specifically, there are several tail-like high heat transfer areas on the channel wall at the downstream of truss rod ends. There are periodic arrow-like low heat transfer areas formed on the channel wall at the downstream of the middle of truss units. It can also be found that the Nu_H on the truss rod surface and channel wall corresponding to the first and second rows of truss units is high. Since the third row of truss units, the Nu_H remains unchanged or slightly drops.

Analysis of flow and heat transfer characteristics

Figure 5 presents the influence of Re_H and β on the flow characteristics of cooling air in the channels filled with *X*-shaped truss array. Figures 5(a) and 5(b) are the distribution of 3-D vortex core in the channels under different Re_H and β. It can be seen from fig. 5(a) that when increasing Re_H, the size of vortex cores around the truss rods becomes smaller, the small vortex cores downstream of the truss rod ends gradually disappear. However, the velocity of vortexes around the truss rods increases significantly as increasing Re_H, especially near the ends of the truss rods. It can be seen from fig. 5(b) that for the channels filled with *X*-shaped truss array at β of 30°, and 45°, the flow field distributions in the channels are similar. For the channels filled with *X*-shaped truss array at β of 60°, the velocity values of horseshoe vortex formed around the truss rods of the first two rows of truss units are high. Then from the third row of truss units, the size and velocity of the vortex around the truss rods of each row of truss units remain basically unchanged. Thus the flow in the channel enters into a periodic state of full development. It can also be found that when increasing β, the horseshoe vortex around the truss rod in the channel gradually becomes larger and the flow becomes more complex, which is caused by the change of the distribution state of the truss rod in the channel at different β. Specifically, with the increase of β, the fluid-flow along the truss rod becomes more intense, and the enlarged elliptical section of truss rod end also brings greater flow disturbance, which leads to the generation of larger horseshoe vortex around the truss rods. Moreover, the increase of β makes the truss rod longer, which results in the decrement of flow section and the increment of blocking area in the channel and may increase the pressure drop of the fluid in the channel.

Figures 5(c) to 5(e) presents the changing trends of f_H along the mainflow direction for the channels filled with *X*-shaped truss array at β of 30°, 45°, and 60°. The horizontal ordinate in figs. 5(c)-5(e) represents the nth row of truss unit ordered from the entrance of the channel. As can be seen, the variation of Re_H does not affect the distribution trend of f_H along the mainflow direction of the channel. For channels filled with *X*-shaped truss array at β of 30° and 60°, the distribution trends of f_H along the mainflow direction are very similar. That is, the f_H of the first row of truss units is very high, the f_H of the second row of truss units decreases rapidly. Then from the second row to the third row of truss units, the f_H of the channel increases slightly, and from the third row of truss units, the f_H of the channel decreases again. The difference is that for the channel with β of 30°, the f_H decreases slowly from the third row to the fifth row of truss units, while the corresponding f_H for the channel with β of 60° decreases rapidly. For the channel with β of 45°, the f_H of the first row of truss units is also very high, and then with the development of cooling flow, the f_H of each row of truss units declines gradually along the mainflow direction. It can also be seen that with the increase of β, the f_H of each row of truss units increases significantly. This is because with the increase of β, the length of truss rod becomes longer, and its flow disturbance effect is enhanced, which increases the f_H of each truss unit region along the mainflow direction of the channel. Additionally, the increase of β reduces

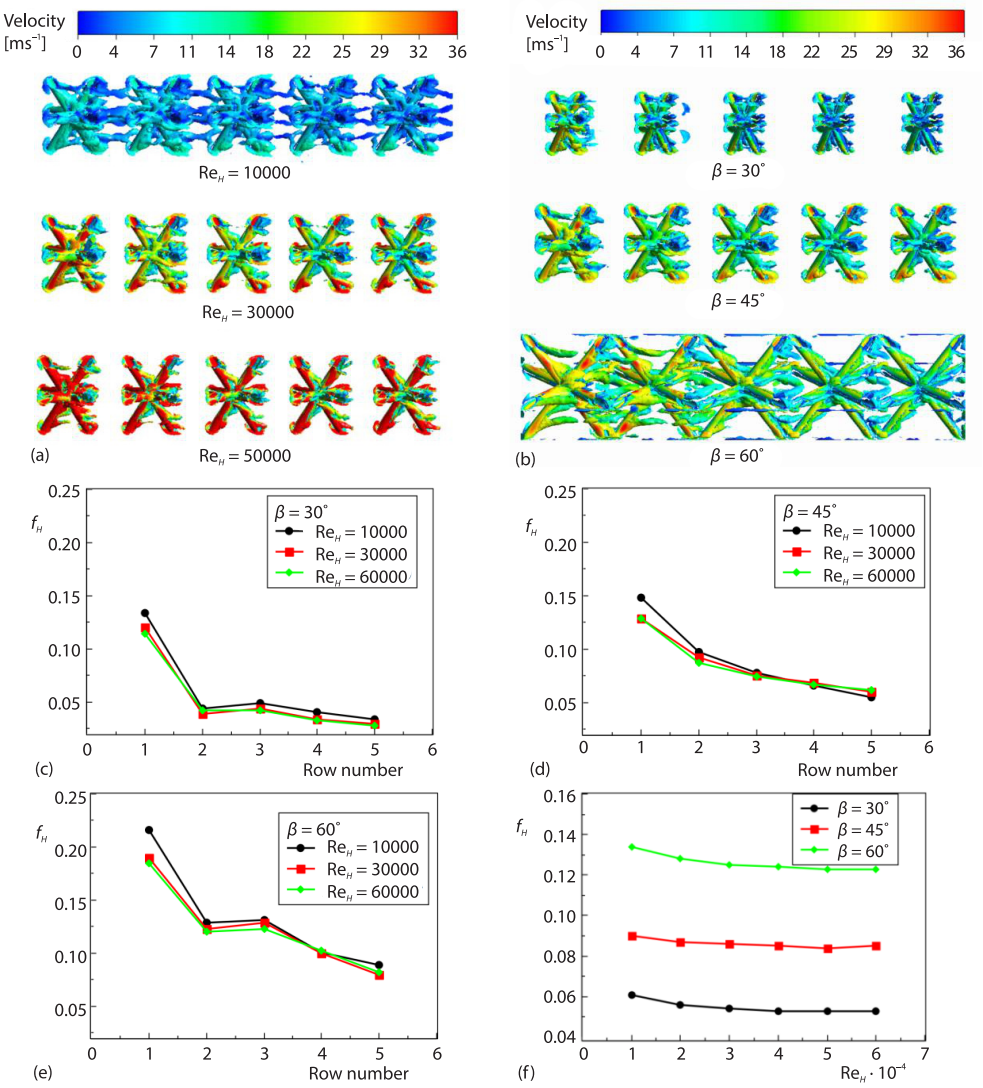

Figure 5. The influence of Re_H and β on the flow characteristics of cooling air in the channels; (a) flow field distribution at different Re_H, (b) flow field distribution at different β, (c) friction coefficient distributions for $\beta = 30°$, (d) friction coefficient distributions for $\beta = 45°$, (e) friction coefficient distributions for $\beta = 60°$, and (f) whole friction coefficient

the flow area of the channel, which also increases the f_H of the channels filled with *X*-shaped truss array.

Figure 5(f) illustrates the change curves of overall f_H along with Re_H for channels filled with *X*-shaped truss array under different β. As can be seen, the overall f_H of the channels filled with *X*-shaped truss array decreases slowly with increasing Re_H. This may be due to the fact that the variation rate of the channel overall pressure difference with Re_H is less than the variation rate of the square of inlet air velocity with Re_H. It can also be found that the increase of β apparently increases the overall f_H of the channel, but the increase rate of f_H with β slightly

decreases. The results also show that the f_H increases by 1.19-1.33 times when β varies from 30-60° at different Re_H, and decreases by 5.6-13.1% when Re_H increases from 10000-60000 at various β.

Figure 6 presents the influence of Re_H and β on the heat transfer characteristics of the channels filled with *X*-shaped truss array. Figures 6(a) and 6(b) displays the distributions of Nu_H on the truss rod surface and channel wall under different Re_H and β. It can be seen from fig. 6(a) that with the increase of Re_H, the Nu_H on the truss rod surface and channel wall both increase greatly. This is because increasing Re_H improves the velocity and turbulence level of cooling air and enhances the flow disturbance effect of the truss rod, which makes the heat transfer effect of truss rod surface and channel wall effectively strengthened. It can be seen from fig. 6(b) that with the increase of β, the Nu_H of truss rod surface and channel wall has been improved. There are two reasons for this phenomenon. Firstly, the increase of β increases the length of the elliptic section long axis of the truss rod, which makes the horseshoe vortex with larger size and faster velocity generate around the truss rod, thus improving the heat transfer effect of the channel wall. Secondly, increasing β makes the truss rod longer, which intensifies the turbulent flow of cooling air in the channel as well as increases the heat transfer area and heat conduction effect of truss rods, thus further strengthening the overall heat transfer effect of the channel.

Figures 6(c)-6(e) shows the distribution curves of row-averaged Nu_H along the mainflow direction for the channels filled with *X*-shaped truss array at β of 30°, 45°, and 60°. The row-averaged Nu_H is the weighted average of Nu_H on the truss rod surface and the corresponding channel wall. It can be seen that due to the entrance effect, the row-averaged Nu_H of the first row of truss unit is the highest. Then, the row-averaged Nu_H of the second row of truss unit decreases rapidly. With the further development of the flow, the cooling air in the channel is gradually heated, and its cooling capacity gradually decreases. Therefore, the row-averaged Nu_H of each row of truss units decreases slowly or remains invariant along the mainflow direction when the row number of truss unit is greater than 3. It can also be found that Re_H has little influence on the variation trend of row-averaged Nu_H of each truss unit region with the row number of truss units. Meanwhile, the increase of Re_H can effectively increase the row-averaged Nu_H of each truss unit region, and improve the heat transfer performance of the channel.

Figure 6(f) demonstrates the change curves of whole-averaged Nu_H with Re_H for the channels filled with *X*-shaped truss array at different β. As shown in fig. 6(f), the whole-averaged Nu_H of the channel increases with increasing Re_H and the rate of increase gradually slows down. It indicates that the effect of increasing Re_H for improving the heat transfer performance of channels filled with *X*-shaped truss array is no longer significant when the Re_H is more than 60000. It can also be found from fig. 6(f) that increasing β can greatly improve the heat transfer performance of channels filled with *X*-shaped truss array, but the increase rate of whole-averaged Nu_H decreases obviously with increasing β. The results of quantitative analysis show that when Re_H increases from 10000-60000, the whole-averaged Nu_H of channels filled with *X*-shaped truss array at β of 30°, 45°, and 60° increase by 1.83, 1.68, and 1.33 times, respectively. When β increases from 30-60°, the whole-averaged Nu_H of the channel increase by 25.4-52.3% under different Re_H.

Figure 7 shows the variation curves of G_H with Re_H and β for the channels filled with *X*-shaped truss array, respectively. As can be seen, the varying trends of G_H with Re_H are similar at different β. Specifically, the G_H increases with increasing of Re_H, and the increase rates all gradually slow down at various β. The results of quantitative analysis show that when Re_H increases from 10000-60000, the values of G_H for the channels filled with *X*-shaped truss array at

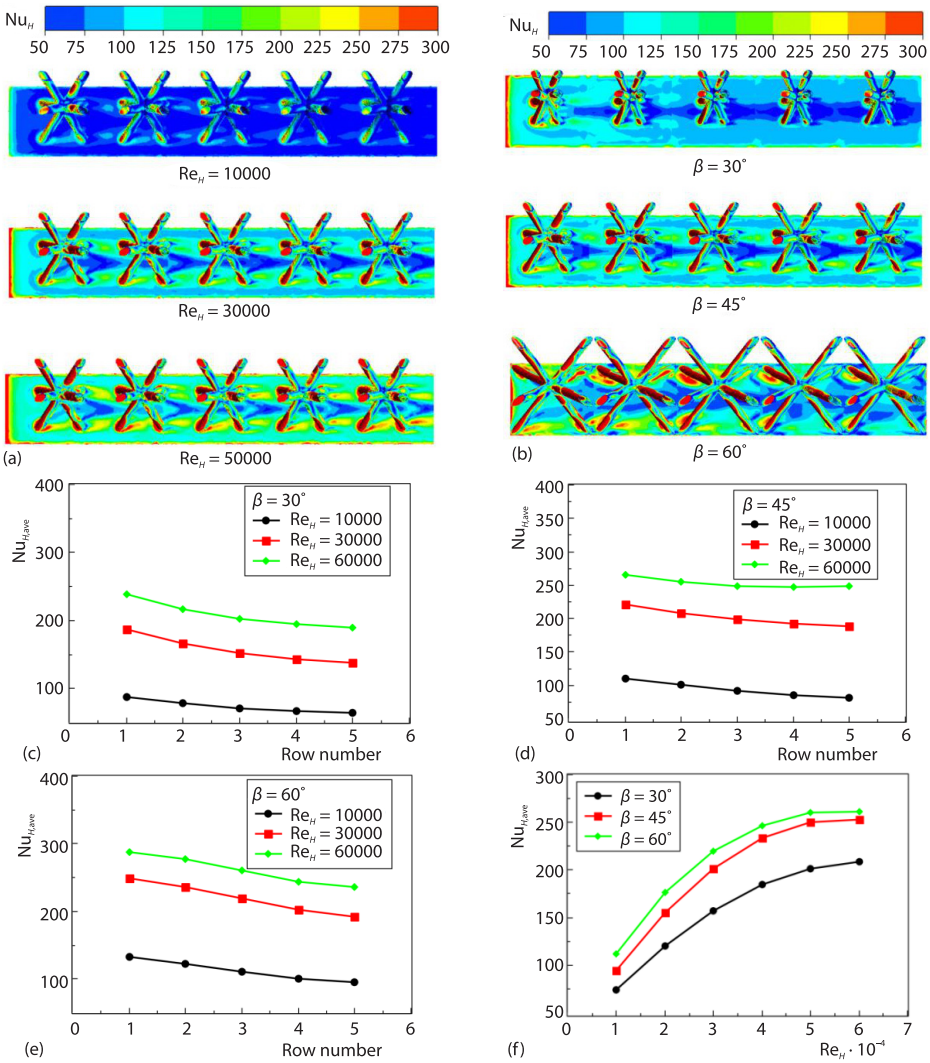

Figure 6. The influence of Re_H and β on the heat transfer characteristics of the channels; (a) local Nusselt number at different Re_H, (b) local Nusselt number at different β, (c) row-averaged Nusselt number for $\beta = 30°$, (d) row-averaged Nusselt number for $\beta = 45°$, (e) row-averaged Nusselt number for $\beta = 60°$, (f) whole-averaged Nusselt number

β of 30°, 45°, and 60° increase by about 1.96, 1.73 and 1.4 times, respectively. According to fig. 7(a) and 7(b), when the Re_H is low, the values of G_H for the channels with β of 45° and 60° are nearly the same, and both are higher than that of the channel with β of 30°. When the Re_H is high, the values of G_H for the channels first increase and then decrease with the increase of β, that is, the G_H for the channel with β of 45° is highest at higher Re_H. In general, the channel filled with X-shaped truss array at β of 45° has a better comprehensive thermal performance at different Re_H. The channel with β of 30° has the worst comprehensive thermal performance at low Re_H, and the channel with β of 60° has the worst comprehensive thermal performance at high Re_H.

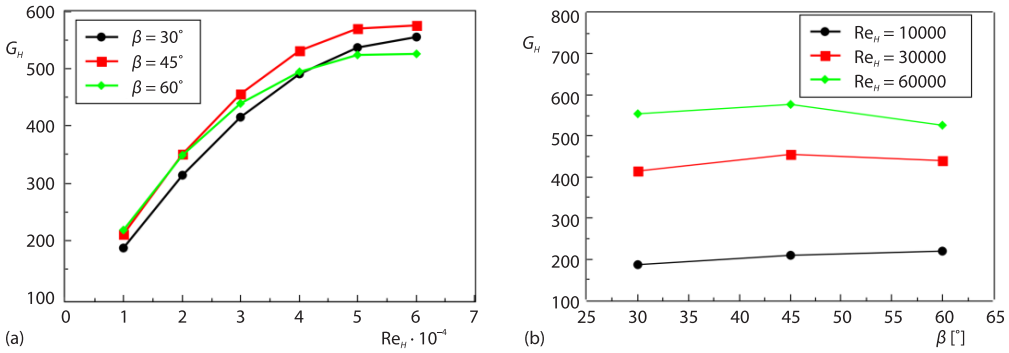

Figure 7. Variation curves of G_H with Re_H and β for the channels; (a) influence of Re_H on G_H and (b) influence of β on G_H

Figure 8 presents the variation curves of the ratios of the heat transfer quantity on the channel wall and on the truss rod surface to the total heat transfer quantity of the channel filled with *X*-shaped truss array at various Re_H and β. It can be seen that, in all cases, the heat transfer quantity of the channel wall is dominant, that is because the area of the channel wall is larger than that of the truss rod surface. The ratio of heat transfer quantity of the channel wall to the total heat transfer quantity of the channel with *X*-shaped truss array ranges from 57.7-77.2%, while the ratio of heat transfer quantity of the truss rod surface to the total heat transfer quantity of the channel with *X*-shaped truss array ranges from 22.9-42.3%. In all cases, the heat transfer quantity of channel wall is about 1.36-3.37 times of that of the truss rod surface. It can also be found that for channels with different β, the increase of Re_H increases the heat transfer quantity of the channel wall and reduces the heat transfer quantity of the truss rod surface. This is because increasing Re_H makes the flow disturbance effect of truss rod end stronger, and then leads to better heat transfer enhancement effect on the channel wall. The increase of β increases the heat transfer quantity of the truss rod surface and reduces the heat transfer quantity of the channel wall. This is because the increase of β increases the area of truss rod surface and improves the heat transfer quantity of truss rod surface. Specifically, when β increases from 30-60°, the heat transfer quantity of channel wall decreases by 9.6-17.8%, and the heat transfer quantity of truss rod surface increases by 30.4-41.9%; when Re_H increases from 10000-60000, the heat transfer quantity of channel wall increases by 9.97-20.97%, and the heat transfer quantity of truss rod surface decreases by 23.15-28.84%.

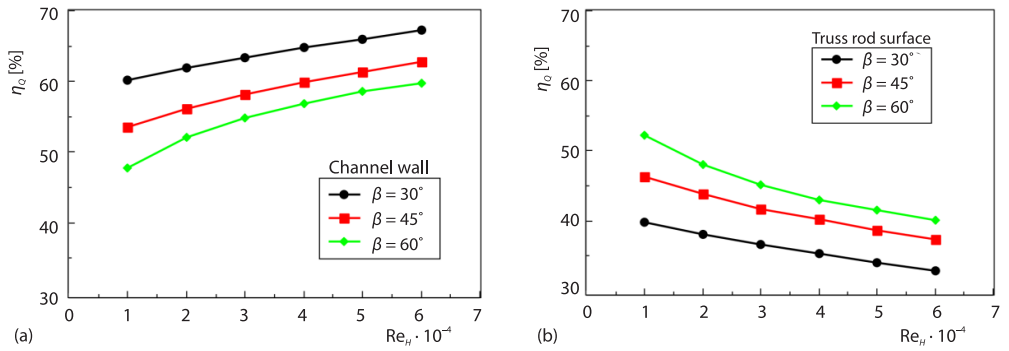

Figure 8. Variation curves of heat transfer quantity with Re_H and β; (a) heat transfer quantity of channel wall and (b) heat transfer quantity of truss rod surface

To confirm the superiority of the *X*-shaped truss array structure in terms of overall cooling performance, the comprehensive thermal performance of *X*-shaped truss array structure and other typical truss array structures (Kagome-type, pyramidal and tetrahedral) were compared in this study. Figure 9 displays the comparison results of the comprehensive thermal coefficients of the previous four kinds of truss array structures at Reynolds number of 30000. As shown in fig. 9, among the four kinds of truss array structures, the *X*-shaped truss array structure has the highest comprehensive thermal coefficient, followed by the Kagome-type truss array structure, and finally the pyramidal truss array structure and tetrahedral truss array structure. This is because the *X*-shaped truss array has the most truss rod ends, which are the dominant factor in the enhancement of the channel wall heat transfer. Specifically, the comprehensive thermal coefficient of *X*-shaped truss array structure is 6.64%, 12.80%, and 19.78% higher than that of Kagome-type truss array structure, pyramidal truss array structure and tetrahedral truss array structure, respectively. Therefore, the *X*-shaped truss array structure studied in this work has the expected good comprehensive thermal performance, and is a promising new cooling structure for the gas turbine blade mid-chord region.

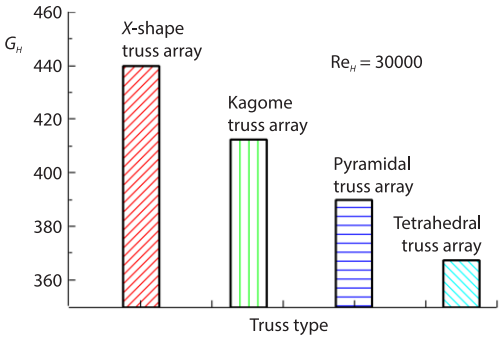

Figure 9. Comparison of comprehensive thermal performance of typical truss array structures

Empirical correlations

At present, there are no flow and heat transfer correlations for the *X*-shaped truss array channels, especially in the case of high Re_H. In this section, the flow and heat transfer correlations about Re_H were fitted firstly for *X*-shaped truss array channels with different β. The power function was used to reflect the relationship between the $Nu_{H,ave}$ or f_H and Re_H of *X*-shaped truss array channels. The correlations can be assumed:

$$f_1 = CRe_H^m \tag{6}$$

where f_1 represents the $Nu_{H,ave}$ and f_H, C, and m are the parameters of the correlations to be fitted.

The fitted parameter values of eq. (9) are shown in tab. 2. The determination coefficients R^2 for $Nu_{H,ave}$ and f_H are greater than 0.91, indicating that the fitting results have high accuracy.

Table 2. The fitted parameter values of flow and heat transfer correlations

β	C for f_H	m for f_H	R^2 for f_H	C for $Nu_{H,ave}$	m for $Nu_{H,ave}$	R^2 for $Nu_{H,ave}$	Re_H
30°	0.316	0.597	0.9826	0.1257	–0.08	0.9144	10000-60000
45°	0.5305	0.5694	0.9688	0.1243	–0.036	0.9229	10000-60000
60°	1.3515	0.487	0.9574	0.209	–0.049	0.9567	10000-60000

Based on the data of this investigation, the correlations that reflect the comprehensive influence of Re_H and β on $Nu_{H,ave}$ and f_H of *X*-shaped truss array channels were also fitted. Ac-

cording to the analysis in section *Empirical correlations*, the Nu_{H_ave} increases monotonously with the increasing Re_H and β; the f_H decreases monotonously with the increasing Re_H, and increases monotonously with the increasing β. Therefore, the power function can be used to fit the correlations among the output parameters Nu_{H_ave} and f_H and the input parameters Re_H and β. The correlations can be assumed:

$$f_2 = a\mathrm{Re}_\mathrm{H}^b\beta^c \tag{7}$$

where f_2 represents the Nu_{H_ave} and f_H, a, b, c are the parameters to be fitted.

The fitting results by the Python module of *curve-fit* are:

$$\mathrm{Nu}_{\mathrm{H,ave}} = 0.2698\mathrm{Re}_\mathrm{H}^{0.4825}\beta^{0.4082} \tag{8}$$

$$f_\mathrm{H} = 0.001388\mathrm{Re}_\mathrm{H}^{-0.04927}\beta^{1.2237} \tag{9}$$

The application ranges of the aforementioned fitted correlations are: $10000 \le Re_H \le 60000$, $30° \le \beta \le 45°$. The maximum prediction deviations of eqs. (8) and (9) for Nu_{H_ave} and f_H are 20.11% and 7.18%. The mean prediction deviations for Nu_{H_ave} and f_H are 6.54% and 1.77%. Those correlations may give a reference for the design of *X*-shaped truss array cooling channels.

Conclusions

In this investigation, the flow mechanisms and heat transfer characteristics of *X*-shaped truss array channels were studied by numerical methods. The main findings are as follows.

- Because of the periodic arrangement of truss units, both the secondary flow vortex in the channel and the Nu_H on the channel walls show periodic distributions along the streamwise direction.
- The row-averaged Nu_H and the f_H of the channel filled with *X*-shaped truss array at various β first decrease quickly and then decrease slowly along the streamwise direction.
- When β increases from 30-60°, the whole-averaged Nu_H and the whole f_H of the channel increase by 25.4-52.3% and 1.19-1.33 times, respectively under different Re_H. The channel with β of 45° has the best comprehensive thermal performance.
- In all cases, the ratio of heat transfer quantity of the truss rod surface to the total heat transfer quantity of the *X*-shaped truss array channel ranges from 22.9-42.3%. Increasing Re_H improves the heat transfer quantity of the channel wall, while increasing β improves the heat transfer quantity of the truss rod surface.

Acknowledgment

This work was supported by the Project Supported by Natural Science Basic Research Plan in Shaanxi Province of China (2022JQ-545), the Project funded by China Postdoctoral Science Foundation (2021M702573) and the National Natural Science Foundation of China (51876157).

Nomenclature

d – truss rod diameter, [mm]
f_H – friction coefficient
G_H – comprehensive thermal coefficient
H – height of the channel, [mm]
L – length of the channel, [mm]
L_s – length of the region of a row truss unit, [mm]
Nu_H – local Nusselt number
$Nu_{H,ave}$ – average Nusselt number
Δp – pressure difference, [Pa]
q – wall heat flux, [Wm^{-2}]
Re_H – Reynolds number
T_f – reference temperature, [K]

T_w – local temperature, [K]
u – inlet velocity, [ms^{-1}]
W – width of the channel, [mm]

Greek symbols

β – inclination angle of truss rod, [°]
δ – thickness, [mm]
λ – thermal conductivity, [Wm^{-1}K^{-1}]
ρ – density of air, [kgm^{-3}]
ν – kinematic viscosity of air, [m^{2}s^{-1}]

References

[1] Tao, Z., *et al*., Aero-Thermal Optimization of a Gas Turbine Blade Endwall with Non-Axisymmetric Contouring and Purge Flow, *Int. J. Heat Mass Tran*., *17*8 (2021), 121626
[2] Zhang, B., *et al*., Experimental Investigation of Flow and Heat Transfer Characteristics on Matrix Ribbed Channel, *Thermal Science*, *24* (2020), 3, pp. 1593-1600
[3] Gasparetto, V. E., *et al*., Multiscale Optimization of Specific Elastic Properties and Microscopic Frequency Band-Gaps of Architectured Microtruss Lattice Materials, *Int. J. Mech. Sci*., *197* (2021), 3, 106320
[4] Liang, D., Mechanical Responses of Ti-6Al-4V Truss Lattices Having a Combined Simple-Cubic and Body-Centered-Cubic (SC-BCC) Topology, *Aerosp. Sci. Techn*ol., *11*6 (2021), 106852
[5] Feng, J., *et al*., Isotropic Octet-Truss Lattice Structure Design and Anisotropy Control Strategies for Implant Application, *Mater. Design*, *203* (2021), 109595
[6] Li, C., *et al*., Architecture Design of Periodic Truss-Lattice Cells for Additive Manufacturing, *Addit. Manuf*., *34* (2020), 101172
[7] Phlipot, G. P., *et al*., A Quasicontinuum Theory for the Non-linear Mechanical Response of General Periodic Truss Lattices, *Journal Mech. Phys. Solids*, *124* (2019), Mar., pp. 758-780
[8] Ye, G., *et al.*, Compression Performances and Failure Modes of 3-D Printed Pyramidal Lattice Truss Composite Structures, *Compos. Commun*., *24* (2021), 100615
[9] Wang, H., *et al*., Foam-filling Techniques to Enhance Mechanical Behaviors of Woven Lattice Truss Sandwich Panels, *Journal Build. Eng*., *40* (2021), 2, 102383
[10] Liu, Y., Mechanical Properties of a New Type of Plate-Lattice Structures, *Int. J. Mech. Sci*., *192* (2021), 106141
[11] Lu, T. J., *et al*., Active Cooling by Metallic Sandwich Structures with Periodic Cores, *Prog. Mater. Sci*., *50* (2005), 7, pp. 789-815
[12] Feng, S. S., *et al*., Thermomechanical Properties of Brazed Wire-Woven Bulk Kagome Cellular Metals for Multifunctional Applications, *Journal Thermophys Heat Tr.*, *26* (2012), 1, pp. 66-74
[13] Qu, Z. G., *et a*l., A Theoretical Octet-Truss Lattice Unit Cell Model for Effective Thermal Conductivity of Consolidated Porous Materials Saturated with Fluid, *Heat Mass Transfer*, *48* (2012), 8, pp. 1385-1395
[14] Wei, K., *et al*., Fabrication and Heat Transfer Characteristics of C/SiC Pyramidal Core Lattice Sandwich Panel, *Appl. Therm. Eng*., *81* (2015), Apr., pp. 10-17
[15] Yan, H., *et al*., Convective Heat Transfer in a Lightweight Multifunctional Sandwich Panel with *X*-type Metallic Lattice Core, *Appl. Therm. Eng.*, *12*7 (2017), Dec., pp. 1293-1304
[16] Zhang, X., *et al.*, Thermo-Fluidic Comparison between Sandwich Panels with Tetrahedral Lattice Cores Fabricated by Casting and Metal Sheet Folding, *Energies*, *1*0 (2017), 7, 906
[17] Jin, X., *et al*., Comparative Evaluations of Thermofluidic Characteristics of Sandwich Panels with *X*-lattice and Pyramidal-Lattice Cores, *Int. J. Heat Mass Trans*., *127* (2018), Part B, pp. 268-282
[18] Bai, X., *et al*., An Analytical and Numerical Estimation of the Effective Thermal Conductivity of Complex Metal Frame Core Structures, *Journal Heat Trans-T Asme*, *14*1 (2019), 2, 024504
[19] Yang, G., *et al*., Comparison of Convective Heat Transfer for Kagome and Tetrahedral Truss-Cored Lattice Sandwich Panels, *Sci. Rep.-UK*, *9* (2019), 1, pp. 1-13
[20] Vaissier, B., *et al*., Par*ametric Design of Graded Truss Lattice Structures for Enhanced Thermal Dissipation, Comput. Aided Design*, *115* (2019), Oct., pp. 1-12
[21] Hou, C., *et al*., Study of Thermo-Fluidic Characteristics for Geometric-Anisotropy Kagome Truss-Cored Lattice, *Chinese J. Aeronau*t., *3*2 (2019), 7, pp. 1635-1645
[22] Ekade, P., *et al*., Fluid-Flow and Heat Transfer Characteristics of Octet Truss Lattice Geometry, *Int. J. Therm. Sci*., *137* (2019), Mar., pp. 253-261
[23] Chaudhari, A., *et al*., Experimental Investigation of Heat Transfer and Fluid-flow in Octet-Truss Lattice Geometry, *Int. J. Therm. Sci*., *14*3 (2019), Sept., pp. 64-75
[24] Kaur, I., *et al*., Endwall Heat Transfer Characteristics of Octahedron Family Lattice-Frame Materials, *Int. Commun. Heat Mass*, *127* (2021), 105522
[25] Mongillo, D. J., *et al*., Gas Turbine Engine Component Having Vascular Engineered Lattice Structure, USA Patent No. 10570746, Patent and Trademark Office, Washington, D. C., USA, 2018

[26] Xu, L., *et al*., Optimization Design of Lattice Structures in Internal Cooling Channel with Variable Aspect Ratio of Gas Turbine Blade, *Energies*, *14* (2021), 13, 3954
[27] Liang, D., *et a*l., Investigating the Effect of Element Shape of the Face-Centered Cubic Lattice Structure on the Flow and Endwall Heat Transfer Characteristics in a Rectangular Channel, *Int. J. Heat Mass Tran*., *153* (2020), 119579
[28] Xi, L., *et al.*, Study on Flow and Heat Transfer Performance of *X*-type Truss Array Cooling Channel, *Case Stud. Therm. Eng.*, *26* (2021), 101034
[29] Xi, L., *et al.*, Cooling Performance Analysis and Structural Parameter Optimization of *X*-type Truss Array Channel Based on Neural Networks and Genetic Algorithm, *Int. J. Heat Mass Tran.*, *186* (2022), 122452
[30] Yang, J., *et al.*, Numerical Simulations and Optimizations for Turbine-Related Configurations, *Thermal Science, 24* (2020), 1, pp. 367-378
[31] Liu, Y., *et al.*, Numerical and Experimental Investigation of a Turbine Guide Vane with Conjugate Heat Transfer Method, *Thermal Science, 26* (2022), 5B, pp. 4259-4269

Paper submitted: March 2, 2022
Paper revised: June 25, 2022
Paper accepted: June 29, 2022